Acoustical classification of benthic habitats in the shallow marine area of the Polish part of the Southern Baltic Sea

Jaroslaw Tegowski, Karolina Trzcinska, Lukasz Janowski

1. Introduction

The study site is located in the shallow marine area of the Polish part of the Southern Baltic Sea in the close neighbourhood of the Rowy harbour at the coast (Figure 1.1). The site is partly located within the nearshore coastal area of Slowinski National Park in northern Poland. The protection of the surrounding marine environments has been established since 1995, when the borders of the National Park were expanded to marine areas up to a depth of 10 m as Ramsar site no. 757. The Rowy site is also located within the area of Natura 2000, no. PLB990002. The area is characterized by low depths, from 4 to 20 m below sea level. Considering its relatively small spatial extent, the geomorphology of the seabed contains crests and valleys of irregular, complex shapes. The bathymetry deepens from south-east to north-west direction covering the main shoal at the centre of the area. This moraine structure is made of boulders and gravels on outcrops of glacial tills partly covered by red algae communities. Large boulders are commonly occupied by dense cover of *Mytilus trossulus* bivalves. The research area is also covered by other substratum outside the glacial tills outcrops, that are: sands, very fine sands, fine sands, sandy gravels and gravelly sands.

The substratum of the study site is made of glacial tills that belong to a large moraine area occurring at the coast. The till outcrops represent relicts of postglacial structures that are crossed by valleys filled with modern marine sand and gravelly sand deposits, which form structures similar to ripplemarks. Glacial tills are often covered by large, dense boulder areas, and such terrain is rare within the Polish part of the southern Baltic Sea. Such a hard substratum provides a good base for various vegetation and benthic communities. Within the immediate surroundings of the Rowy area there is a lack of big urban or industrial areas, sources of contamination, and big river estuaries, so the environment maintains its relatively original nature. Previous research has confirmed the high biodiversity of the benthic communities within the analysed area (Tegowski et al. 2009). The presence of six species of red algae has been found there, such as Bangiophyceae, which is very rare in the Polish coast of the Baltic Sea, including unique Furcellaria lumbricalis and Polysiphonia fucoides. Moreover, boulder sites are often colonized by dense, cemented communities of Mytilus trossulus bivalves, with over 2500 individuals per m^2 in some locations (Kendzierska, 2009). The presence of large patches of such macroalgae is very valuable in terms of the functioning of the ecosystem and increasing the diversity of the phytophile fauna (Maritime Institute in Gdansk, 2006).

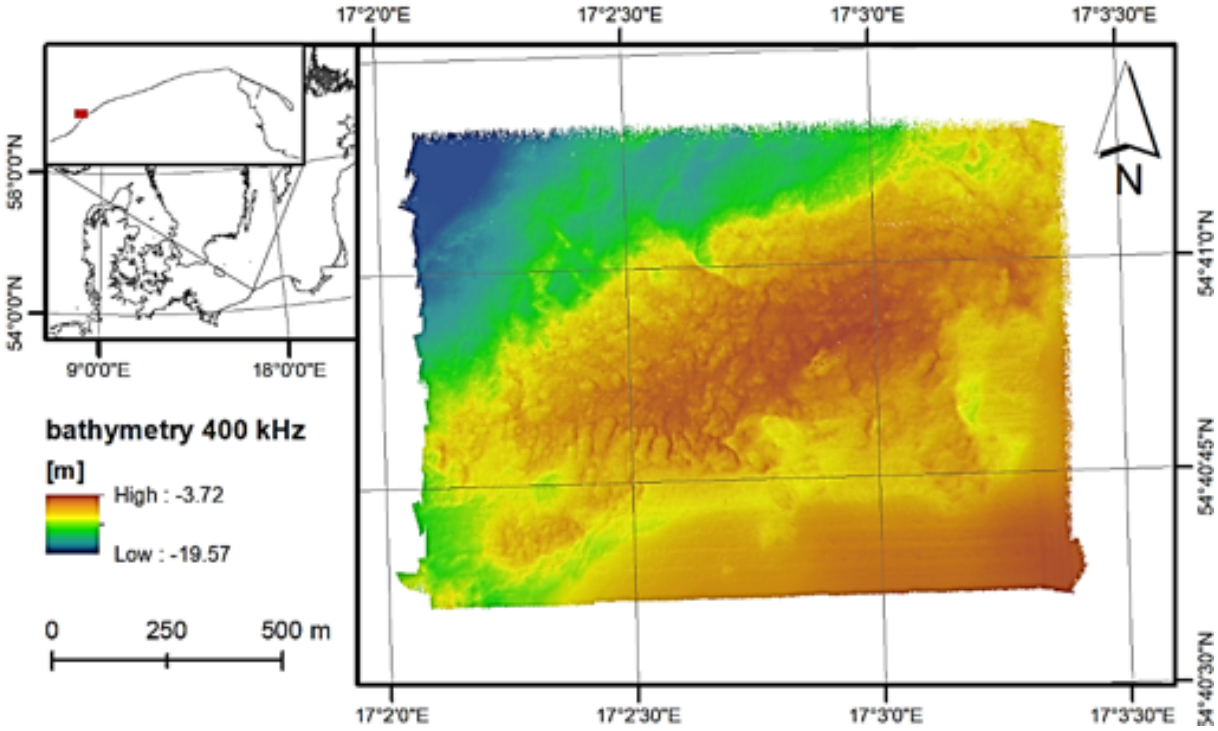

Figure 1.1. Site location within the Polish coast of the Baltic Sea (left), bathymetry of the area generated from 400 kHz MBES measurements (right).

2. Two-dimensional Fourier analysis of the corrugated bottom surface

In the ECOMAP project, the 2D FFT method was used to analyse the bottom forms of the studied southern Baltic Sea area. A novelty is the calculation of spectral parameters, such as spectral moments, spectral width, skewness and kurtosis of the spectrum and the average frequency. Some of the parameters well reflect the morphological features of the bottom surface and are helpful in its classification. In Matlab's software environment, a computational algorithm for two-dimensional spectral analysis of the seabed surface has been developed and its subsequent steps have been tested. In the first step, a regular sinusoidal surface of the bottom with spatial parameters corresponding to large sand waves was generated (Fig. 2.1).

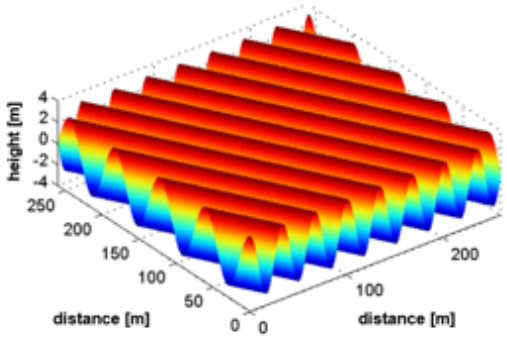

Figure 2.1. Artificially generated regular sinusoidal surface.

In order to obtain a comprehensive information about the parameters of rough bottom surface, a 2D FFT of its surface height model was carried out using the following expression:

$$P(K_x, K_y) = \int_{+\infty}^{-\infty} \int_{+\infty}^{-\infty} s(x,y) e^{-i2\pi(K_x x, K_x y)} dxdy, \quad (2.1)$$

where: K_x i K_y are spatial frequencies expressed as cycle·m^{-1}. The result of the transformation is a normalized spatial spectrum of the surface height presented in Figures 2.2 a) and b).

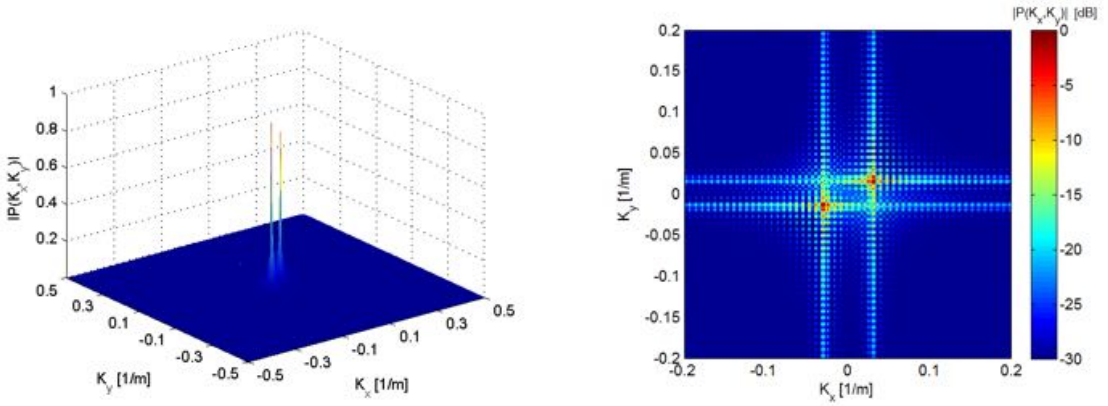

a) b)

Fig. 2.2. a) Normalized two-dimensional spectrum of the sinusoidal surface, b) the normalized two-dimensional spectrum of the sinusoidal Surface - projection on the K_x-K_y plane.

Fig. 2.2. b) shows perpendicularly to each other linear structures of the spectrum resulting from its leakage. In the later steps the spectral window will be applied significantly limiting this effect.

Another approximation of the natural surface of the bottom is the generated artificial surface with randomly distributed heights of normal distribution - Figures 2.3 a) and b).

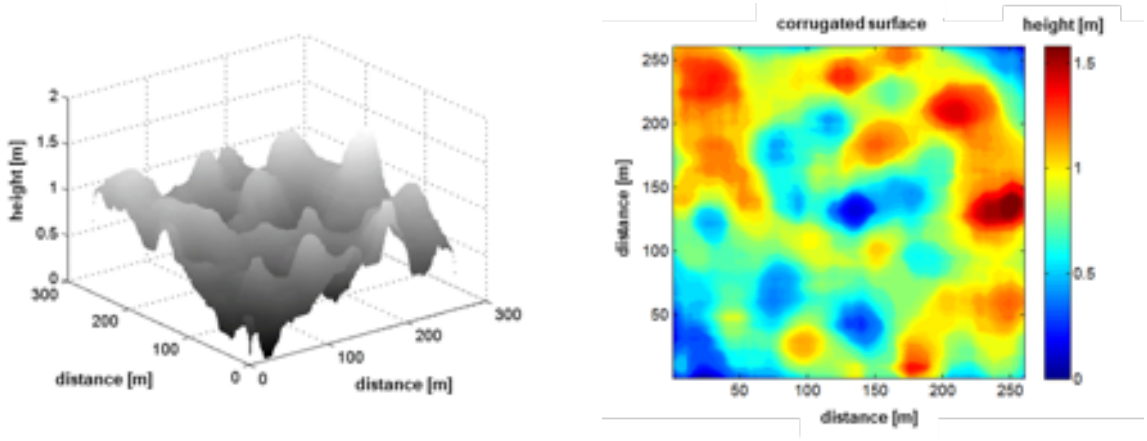

a) b)

Figure 2.3. a) Synthetic bottom surface with randomly distributed heights and normal distribution, b) projection in x-y plane of a synthetic bottom surface with randomly distributed heights with normal distribution.

Before the calculation of the spectrum of the surface, the average height of the surface was subtracted from it and then the procedure of removing the trend, i.e. the average slope of the entire surface, was carried out. The result of such transformation is the surface shown in Fig. 2.4 a). The normalized 2D FFT of the transformed surface is shown in Fig. 2.4 b). Also in this case the leakage of the spectrum is visible.

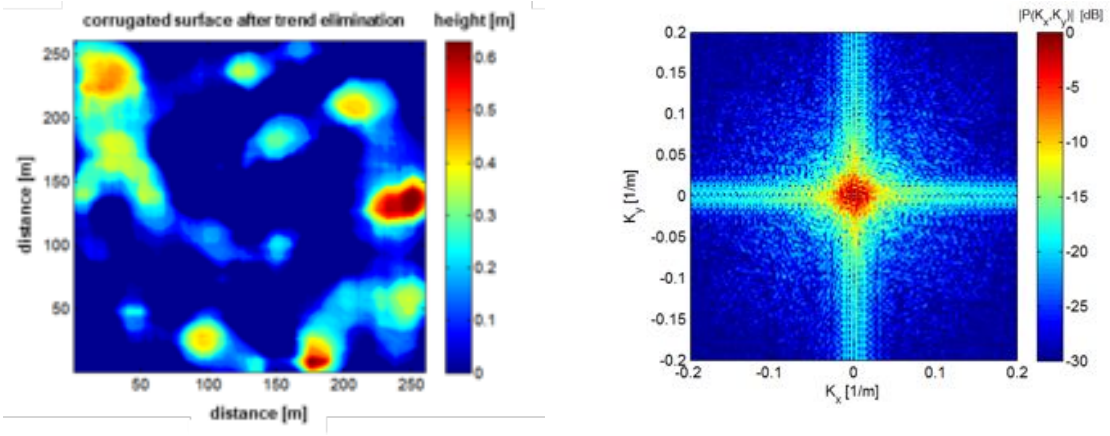

a) b)

Fig. 2.4. a) Synthetic surface of the bottom after removing the average height of the bottom and removing the average slope of the surface (trend), b) projection into the KxKy plane of the normalized two-dimensional spectrum of the synthetic surface of the bottom, from which are subtracted its average height and the trend is removed.

The third approach to the bottom surface is the bathymetric model (Figures 2.5 a) and b)) obtained by summing up the sinusoidal surface (Figure 2.1) with a surface of randomly distributed heights of normal distribution (Fig. 2.3 a)) multiplied by the scaling factors.

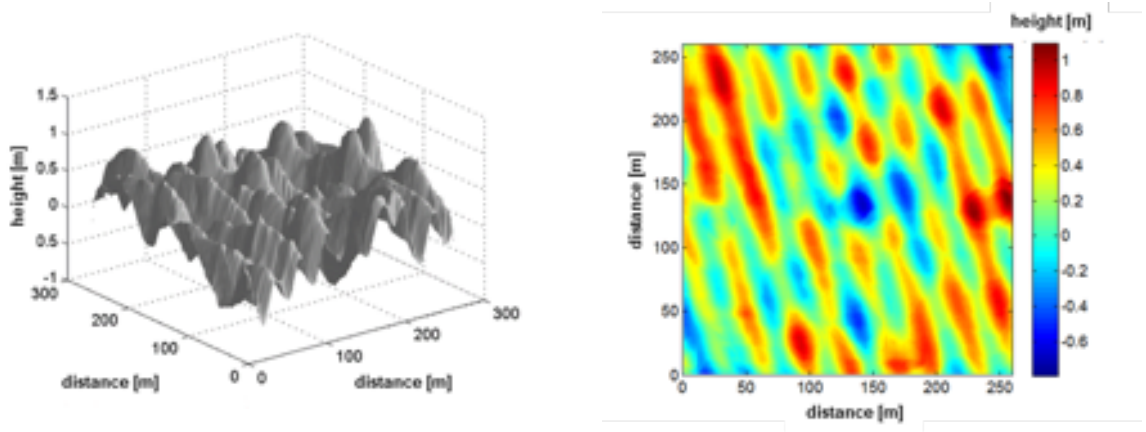

a) b)

Fig. 2.5. a) Synthetic bottom surface with the sand waves structure, b) projection on an x-y plane of a synthetic bottom surface with a sand wave structure on it.

The normalized spectrum of the surface constructed in such a way is shown in Fig. 2.6 a). The line connecting symmetrically distributed spectrum maxima determines the direction of the wavy structure

of the bottom. Characteristic, perpendicular to each other linear structures of the spectrum leakage require the use of a procedure of their filtration. For this purpose, the synthetic surface of the bottom was multiplied by a two-dimensional spectral window, which is a function selected from a number of functions called Discrete Prolate Spheroidal Sequences (DPSS). In our case, we used the first order function and the window width parameter NW = 2 (NW - Slepian bandwidth parameter) Fig. 2.6.b.

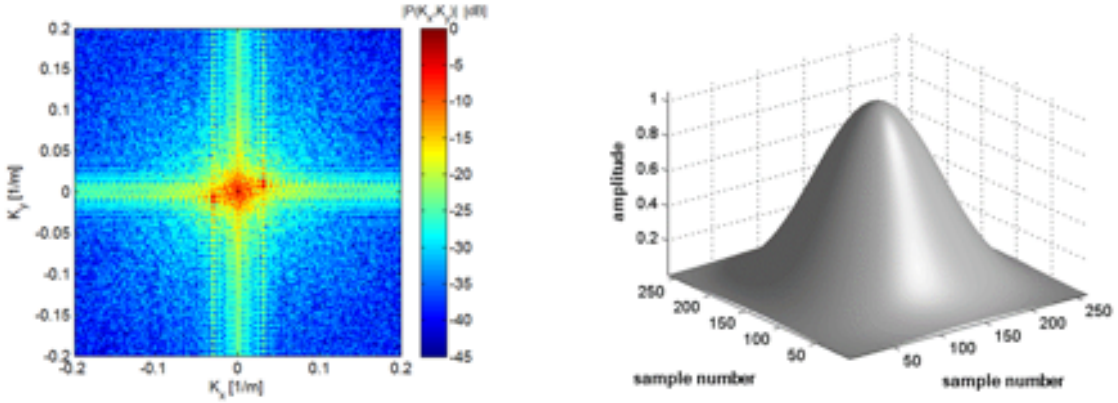

a) b)

Fig. 2.6. a) Projection of the standardised two-dimensional spectrum of the synthetic bottom surface with sand waves structure on the K_x-K_y plane, b) two-dimensional spectral window as a function selected from a series of Slepian Sequences (first order window, NW = 2).

The result of multiplication of the DPSS spectral window by the surface is a new synthetic bottom surface, as shown in Figures 2.7.a and 2.7.b.

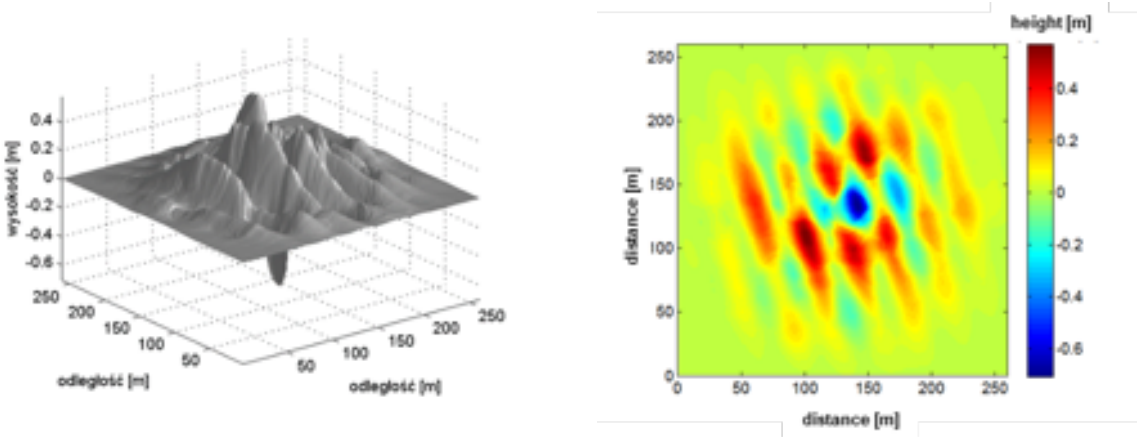

a) b)

Fig. 2.7. a) Synthetic bottom surface created by multiplication of the artificial surface (Fig 1.8) by the DPSS spectral window function, b) projection in x-y plane of the synthetic bottom surface from Fig 2.7 a).

In this way, the transformed bathymetric model of the surface was subjected to a 2D FFT, the result of which is the spectrum presented in Fig. 2.8. The line connecting the maxima of the spectrum determines the direction of morphological structures of the bottom.

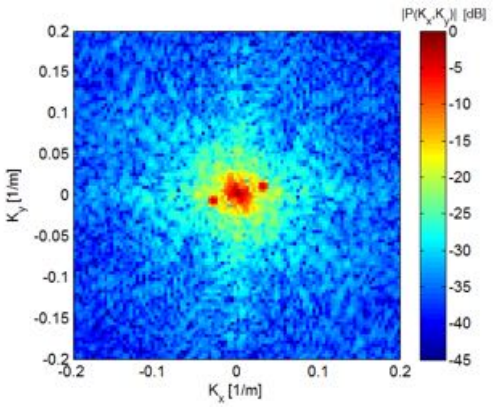

Fig. 2.8. Projection of the standardised two-dimensional spectrum of the synthetic bottom surface from Fig. 2.7 into the K_x-K_y plane.

2.2. 2D FFT algorithm of the corrugated bottom surface of the Rowy testing area

The above example of the application of 2D FFT to characterization of synthetic rough surfaces was applied to a model of digital bathymetry of the bottom registered with a multibeam echosounder. The result of the subsequent steps of the algorithm is the calculation of the spectra in the sliding window and then the spectral parameters characterizing the rough surface of the bottom and forming an input dataset to the algorithms of classification of morphological forms of the bottom (Tegowski et al. 2016).

An example of the work of algorithm are its successive steps presented for the test data set of real bathymetric data from the bottom of the Rowy area (Fig. 2.9), characterized by a diversified relief. After subtracting the average height and removing the trend, the transformed image of the bottom height was obtained (Fig. 2.10).

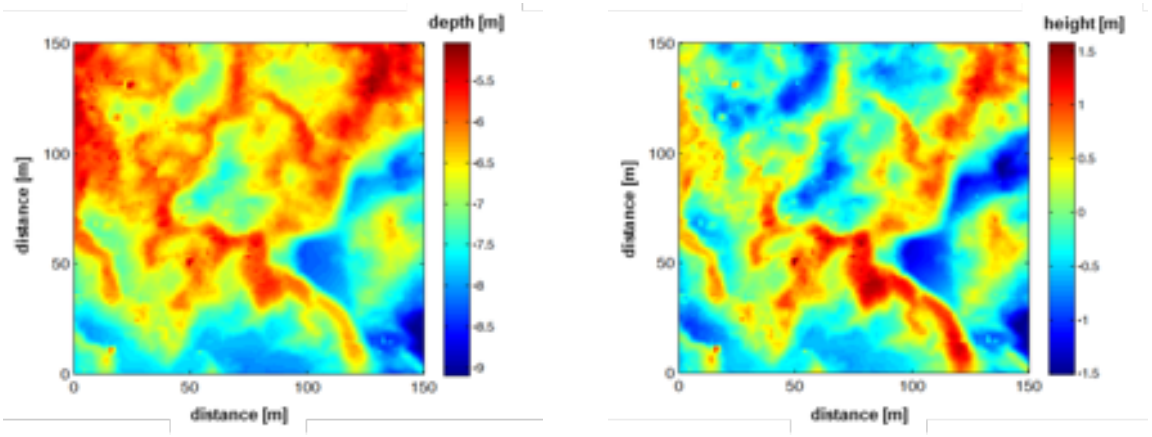

a) b)

Fig. 2.9. a) Bathymetric image of the Rowy area fragment, b) picture of the height of the bottom of the Rowy area fragment after removing the average height and removing the trend.

In the next step, in order to reduce the effect of spectrum leakage after the 2D FFT transformation, the bathymetric surface was multiplied by the DPSS spectral window function. The obtained surface was subjected to Fourier transformation. The result of the operation is shown in Fig. 2.10.b.

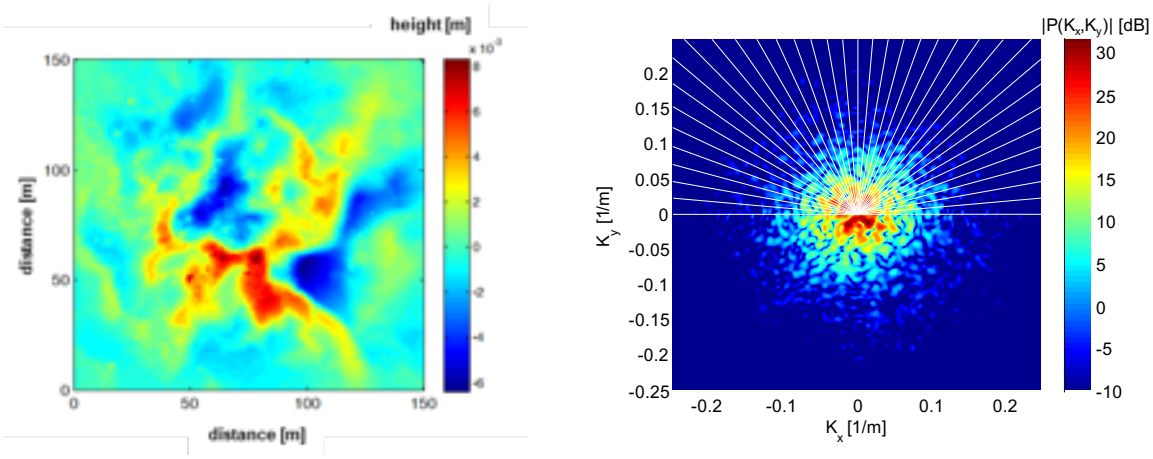

a) b)

Fig. 2.10. a) Projection in x-y plane of a fragment of the area of the bottom surface of the Rowy area created by multiplying the area by the DPSS spectral window function, b) projection on the K_x-K_y plane of the two-dimensional spectrum of the transformed fragment of the area.

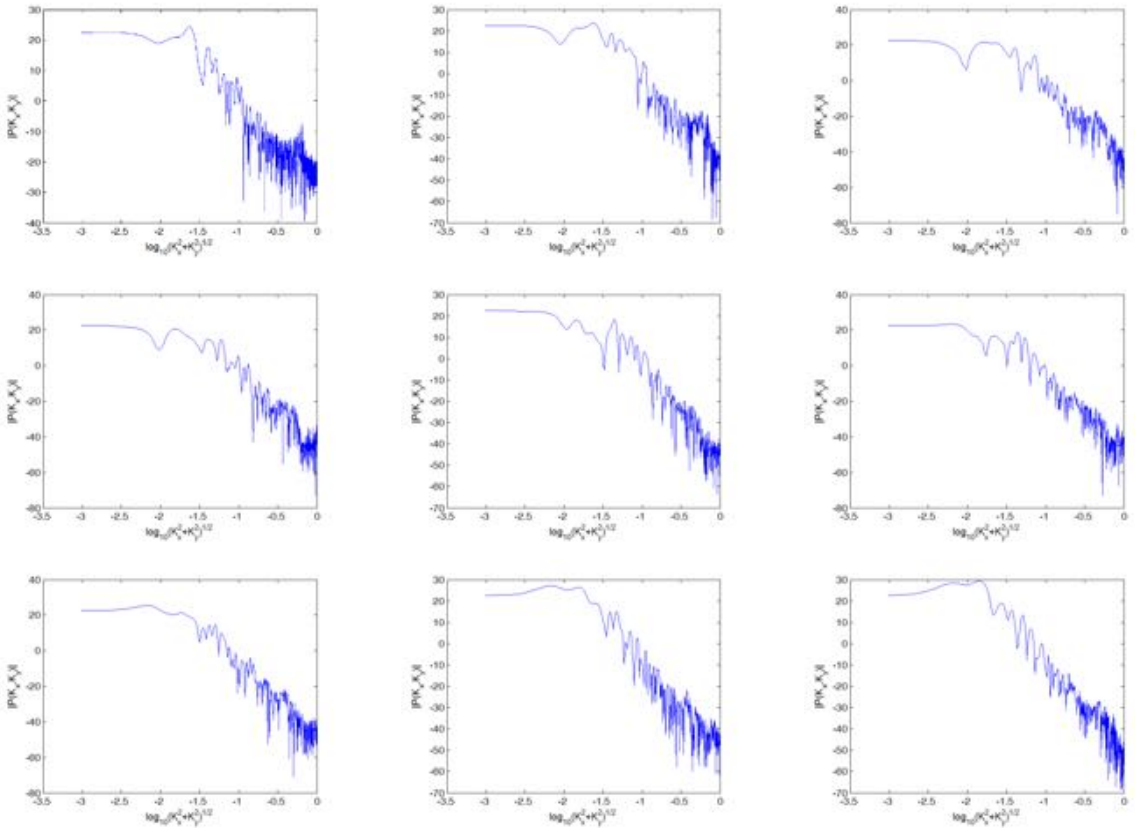

Fig. 2.11. Example of consecutive one-dimensional spectra separated from the two-dimensional spectrum in Fig. 2.10.b for cutting angles from 0 to 45°.

In the next stage of the spectral analysis, one-dimensional cross-sections from 0 to 180° every 5° were separated from the two-dimensional surface spectrum (Fig. 2.10.b). Fig. 2.11 shows 9 consecutive one-dimensional spectra for angles from 0 to 45° respectively.

2.3. Parameterisation of the one-dimensional spectra

In order to find the particular features of the examined bottom surfaces, the one-dimensional spectra were parameterized. For each of the 37 spectra, spectral moments m_r defined as (Clough and Penzien, 1975):

$$m_r = \int_{-\infty}^{+\infty} \omega^r S(\omega), \tag{2.2}$$

where: r is the moment order, ω - angular frequency and $S(\omega)$ – power spectral density. The mean frequency is defined as:

$$\omega_0 = \frac{m_1}{m_0}. \tag{2.3}$$

Spectral widths are calculated according to the formulas:

$$v = \frac{m_0 m_2}{m_1^2} - 1, \quad r = 0, 1, ..., 7 \tag{2.4}$$

and

$$\varepsilon^2 = \frac{m_0 m_4 - m_2^2}{m_0 m_4}. \tag{2.5}$$

They are defined as the concentration of the spectral energy density around the average frequency ω_0. A very sensitive parameter for changes in surface shape is the spectral skewness defined for the central moments as:

$$\gamma_s = \frac{\tilde{m}_3}{\tilde{m}_2^{3/2}}. \tag{2.6}$$

Spatial distributions in the form of maps of calculated spectral parameters present characteristic features of the bottom relief of the studied area. They also serve as an input dataset to the algorithms of classification of morphological forms of the bottom.

3. Materials and methods

3.1 Data acquisition and processing

Multibeam echosounder datasets were acquired using a NORBIT iWBMS (model STX) system mounted on a portable pole at the 'Zelint' motorboat. The MBES device was manufactured especially for shallow marine areas and is typically dedicated for hydroacoustic measurements from 0.2 to 160 m below sea level. At a maximum frequency of 400 kHz, the receiving beam width is 0.9° x 0.9° and allows the collection of 512 beams. This multibeam echosounder has an integrated WaveMaster GNSS/INS (Global Navigation Satellite Systems / Inertial Navigation System) that was supported by RTK-GPS (Real Time Kinematic / Global Positioning System) corrections for precise positioning and attitude measurements. Using the ASG-EUPOS NAWGEO service (www.asgeupos.pl), we received real-time positioning with an accuracy of 3 cm horizontally and 5 cm vertically. In this study the influence of acoustic absorption on the recorded signals was ignored but were considered it in the post-processing. For the purpose of this research, the frequency was set either to 150 kHz or 400 kHz, whereas the swath range covered 150-160°. The maximum ping rate for both frequencies was 20 Hz, we applied a 200 μs for 150 kHz and 500 μs for 400 kHz frequency modulated chirp, with a bandwidth of 6 and 80 kHz, respectively. Surveys were designed with respect to the systematic collection of five sound velocity profiles and a constant vessel speed of 2.83-3,09 m/s.

Multibeam echosounder datasets were processed using QPS Qimera 1.6.3 and Fledermaus Geocoder Toolbox 7.8.4 software allowing bathymetry and backscatter data processing, cleaning and mosaicking. After registration, a patch test has been applied. A bathymetric grid with pixel size of 0.25 x 0.25 m was calculated for both frequencies. Because we did not find any significant differences in MBES measurements recorded at 150 kHz and 400 kHz, we combined both frequencies to obtain bathymetry from dense point cloud. Qimera software allowed for manually cleaning of outliers and acoustic spikes. Backscatter grids were generated based on beam time series (snippets) with a resolution of 0.5 m for 400 kHz and 0.75 m for 150 kHz using a mosaicking method with Angle Varying Gain (AVG) correction of the angular dependency included in the Geocoder engine (Fonseca et al. 2009). We applied the default settings of AVG (Angle Varying Gain): 'flat' mode, 'blend' mosaicking style, and '300' size of processing window. AVG is commonly used method for correction of MBES angular dependency and obtain normalized seafloor backscatter dataset. The standard type of AVG is 'flat' mode, responsible for reducing backscatter signal noise and smoothing its fine variations. "Blend' mosaicking style is responsible for management of overlapping MBES swaths. This type of the method allows to allows to blend the pixels along the nadir ship track line with other overlapping pixels (Schimel et al., 2018). Window size corresponds to a specific number of consecutive MBES pings considered for AVG

correction (see e.g. Parnum and Gavrilov, 2011). All MBES datasets were extracted as surface floating point files in UTM 33N projected coordinate system.

Table 1. List of bathymetry and backscatter features extracted in this study.

ID	feature of bathymetry	window size	ID	feature of backscatter	scale of objects
1–4	standard deviation	3 x 3, 5 x 5, 7 x 7, 9 x 9	40	standard deviation	1–20
5–8	kurtosis	3 x 3, 5 x 5, 7 x 7, 9 x 9	41	GLCM Homogeneity	1–20
9–12	VRM ruggedness	3 x 3, 5 x 5, 7 x 7, 9 x 9	42	GLCM Entropy	1–20
13	slope	3 x 3	43	GLCM Contrast	1–20
14	variance	3 x 3	44	GLCM Standard Deviation	1–20
15	curvature	3 x 3	45	GLCM Dissimilarity	1–20
16	profile curvature	3 x 3	46	GLCM Correlation	1–20
17	planar curvature	3 x 3	47	GLCM Angular Second Moment	1–20
18	aspect	3 x 3	48	GLCM Mean	1–20
19	eastness	3 x 3			
20	northness	3 x 3			
21	surface area to planar area (arc-chord ratio)	3 x 3			
22	BPI 50	3 x 3			
23	BPI 250	3 x 3			
24–25	fractal dimension (Dfft)	20 x 20, 35 x 35			
26–27	spectral moment m_0	20 x 20, 35 x 35			
28–29	spectral moment m_2	20 x 20, 35 x 35			
30–31	mean frequency (ω_0)	20 x 20, 35 x 35			
32–33	spectral width (v^2)	20 x 20, 35 x 35			
34–35	spectral skewness ($\widetilde{\gamma_s}$)	20 x 20, 35 x 35			
36–37	Quality factor (Q-factor)	20 x 20, 35 x 35			
38–39	spectral skewness defined for central moments (γ_{s_centr})	20 x 20, 35 x 35			

We employed the general workflow for benthic habitat mapping from Janowski et al (2018) to the MBES data. Hence, we extracted statistical and geomorphometric features of bathymetry (i.e. slope, vertical ruggedness measure (VRM; Sappington et al. 2007), bathymetric position index (BPI; Wilson et al. 2007)), as well as textural features of backscatter (different types of grey level co-occurrence matrices (GLCMs; Haralick 1973)). In addition, we derived first and second order 2D spectral

parameters of bathymetry. A list of all extracted features is presented in Table 1. Features 1-23, were created using the Benthic Terrain Modeler toolbox in ArcGIS (Walbridge et al. 2018), features 24-39 were calculated using algorithms coded in Matlab, and features 40-48 were created using OBIA workflows in Trimble eCognition software (Janowski et al. 2018). If possible, we tested various sizes of rectangular moving windows or scales of image-based objects (Table 1). It enabled us to perform multi-scale analysis of geospatial datasets to a certain extent (Misiuk et al. 2018).

3.2 Ground truth data acquisition and processing

Ground-truth samples were acquired with a Remotely Operated Vehicle (ROV) and a Van-Veen grab sampler. Based on previous research in this area and backscatter acoustic characteristics, their locations were carefully chosen in representative way to catch all properties of the seabed (Tegowski et al. 2009). ROV video recordings were collected in more than half of the sites, allowing to investigate the locations and surrounding areas. Sediment samples were collected in 46 sites and they were classified using Folk and Ward and Wentworth systems (Folk & Ward 1957; Wentworth 1922).

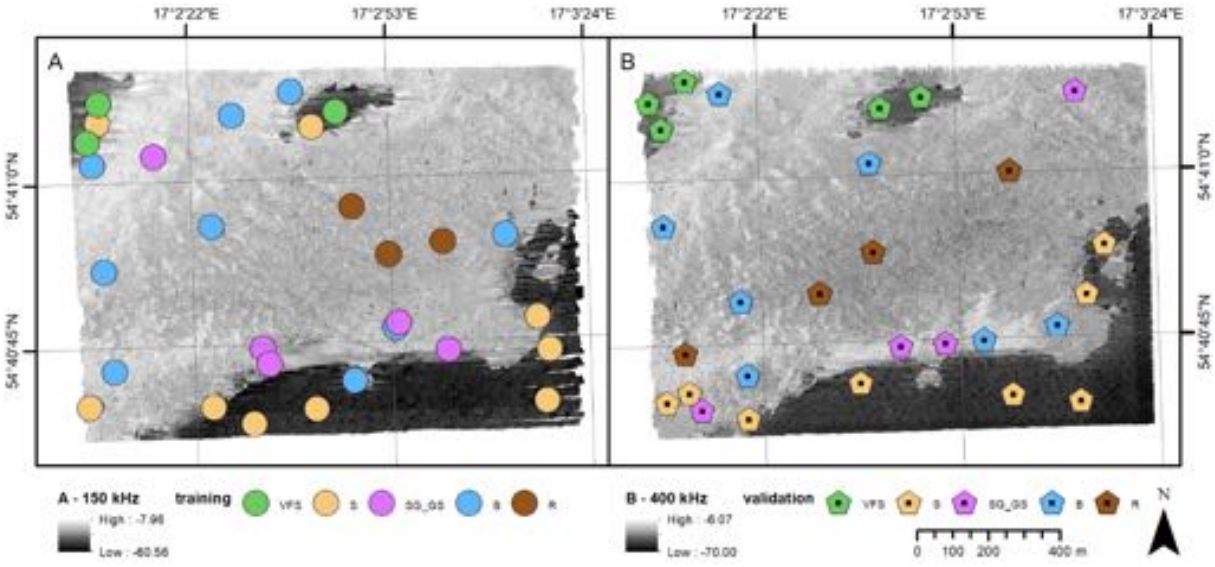

Fig. 3.1. Locations of ground-truth training and validation samples on MBES backscatter image for A - 150 kHz and B - 400 kHz frequencies. S - sand, B - boulders, R - red algae on boulders, SG_GS - sandy gravel or gravelly sand, VFS - very fine sand.

From 57 ground-truth samples, 29 were chosen for training of supervised classifiers, whereas 28 were used to test classification performance. The split was performed based on traditional, random single-split. Our separation for training/test samples was targeted to obtain better prediction performance than model fitting. Locations of ground-truth samples used for training and validation with reference to MBES backscatter are presented in Figure 3.1. Note, that the class of artificial structures (A) is omitted in the Figure 2 due to its presence in one, certain site of the area. It was therefore classified manually at the end of supervised classification process, based on the exact location of the shipwreck visible on MBES bathymetry and ROV video datasets.

3.3 Image analysis for predictive habitat mapping

To evaluate the importance of individual features, the Boruta feature selection algorithm (Kursa & Rudnicki 2010) was applied, which is based on the random forest machine learning algorithm by Breiman (2001). The algorithm belongs to wrapper feature selection methods that evaluate the performance of a certain model after searching for all possible feature selections. Usually, wrappers aim is to minimise prediction error and because of that, they may belong to common minimal-optimal methods (Kursa, 2016). The wrapper was implemented in R using the 'Boruta' and 'rgdal' libraries. The mentioned wrapper method iteratively evaluated sets of different input features and calculate the Z-score, which is indicative for feature importance. Each evaluation is done by introduction of other, irrelevant features that are treated as a reference for assessment of original features. Z-score is calculated based on random forest method during training of the classifier (Breiman, 2001). Based on the feature importance measure, feature selection is performed iteratively successively removing irrelevant features. In order to exclude tentative (unallocated) features, the maximum number of Boruta iterations was set to 5000. Although our aim was to identify all relevant features, including weakly relevant ones (Nilsson et al., 2007), we allowed the possibility of refinement if some of them would be correlated with each other. To get rid of highly correlated features, a correlation analysis was performed in R software using 'caret' package. Features with absolute Pearson's correlation of 0.75 or higher were removed.

We applied an object-based image analysis (OBIA) in this study. We used the Trimble eCognition software for OBIA. The aforementioned image processing techniques were invented in the 2000's to manage an increasing number of high-resolution remote sensing images containing larger amount of heterogenous information (Blaschke 2010). Through a multiresolution segmentation (MS) algorithm, OBIA merges similar pixels of an image into groups of uniform shapes and sizes (Benz et al. 2004). Multiresolution segmentation has some parameters that we defined and tested to generate meaningful image objects. While colour parameter correspond to relative values of MBES backscatter intensity, the associated parameter, shape is related to the ratio between compactness and smoothness. Compactness refer to the ratio between the segment border length and the square root of the pixel count within it. Smoothness is related to the ratio between the border length of segment and its bounding box (Benz et al. 2004). Both weighted pairs of parameters may be determined by 0.1 to 0.9 values, whereas the total value of each pair is 1. MS parameters of shape and compactness were defined to 0.1 and 0.5, respectively. We tested also 1-20 scale parameters of MS, responsible for termination of image objects merging process. Segmentation was performed to delineate image objects based equally on two backscatter derivatives: 150 and 400 kHz.

Similarly like in other benthic habitat mapping studies, a few supervised classification approaches were tested to generate predictive outcomes based on ground-truth samples (Diesing et al. 2014; Hasan

et al. 2012; Montereale Gavazzi et al. 2016). In this study they include classification and regression trees (CART), support vector machines (SVM), random forest (RF) and k-nearest neighbours (KNN). We used implementation of these algorithms available in the eCognition software. The aim of CART classifier is to find a logical separation between classes in an explicit manner. The algorithm creates a decision tree that is associated with a system of questions and answers allowing to find the final classification (Breiman et al., 1984). Support vector machines based on machine learning technique is an algorithm that transforms datasets into a multidimensional feature space in order to find the appropriate boundary between them. Data points are called vectors, and those that support border selection are called support vectors. Machine learning models that use support vectors are called support vector machines (Cortes and Vapnik, 1995). Random Forest is the machine learning method for classification, regression and other tasks, which consists of constructing multiple decision trees generating the class dominant or predicted average of individual trees (Breiman, 2001). K-nearest neighbours classify a specified object (query point) by a certain number (K) of known training samples that are located at the nearest neighbour around the query point. Euclidean distances between the object and each instances are calculated in feature space to estimate influence area of the neighbours. The KNN classification algorithm was described in details in the Bremner et al. (2005).

We used validation ground-truth samples to create error matrices and calculate accuracy assessment statistics (Foody 2002). These include user's and producer's accuracy (Congalton 1991; Story & Congalton 1986), overall accuracy and kappa index of agreement (KIA; Cohen 1960).

4. Results

4.1 Ground-truth data processing

Six benthic habitat classes were determined: VFS - very fine sands with traces of worm burrows, S - sands with ripple marks, SG_GS - sandy gravels or gravelly sands, B - boulders covered by high density of *Mytilus trossulus* bivalves, R - boulders covered by *Mytilus trossulus* bivalves and additionally overgrown by red algae, A - artificial structures. Extensive identification of benthic habitats with their reference to MBES backscatter in this area was described in Janowski et al (2018).

4.2 Feature selection

The results of the Boruta feature selection are presented in Figure 4.1. The algorithm performed 612 iterations and confirmed 11 important features. The most important feature in this study was 400 kHz backscatter followed by backscatter 150 kHz, fractal dimension (35), fractal dimension (20), spectral skewness defined for central moments (20), *Q*-factor (35), spectral skewness (35), bathymetry, spectral

moment m_0 (35), spectral width (35), spectral moment m_2 (35). Boruta results indicate that some spectral parameters have a higher importance than bathymetry, from which they were derived. This is especially visible in fractal dimension parameter, which importance was about twice as high than bathymetry. Noteworthy, all other extracted features, including geomorphometric, statistical and textural features of MBES bathymetry and backscatter were not been considered as important. Our initial results suggest relevance of multi-frequency MBES, i.e. the first and second most important features were backscatter collected with different frequencies. Correlation analysis allowed to remove 6 highly correlated features, like following: spectral skewness – 35, fractal dimension – 20, fractal dimension – 35, spectral width-35, spectral moment m_0 – 35, backscatter 150 kHz. Correlation matrix was shown at Figure 4.2.

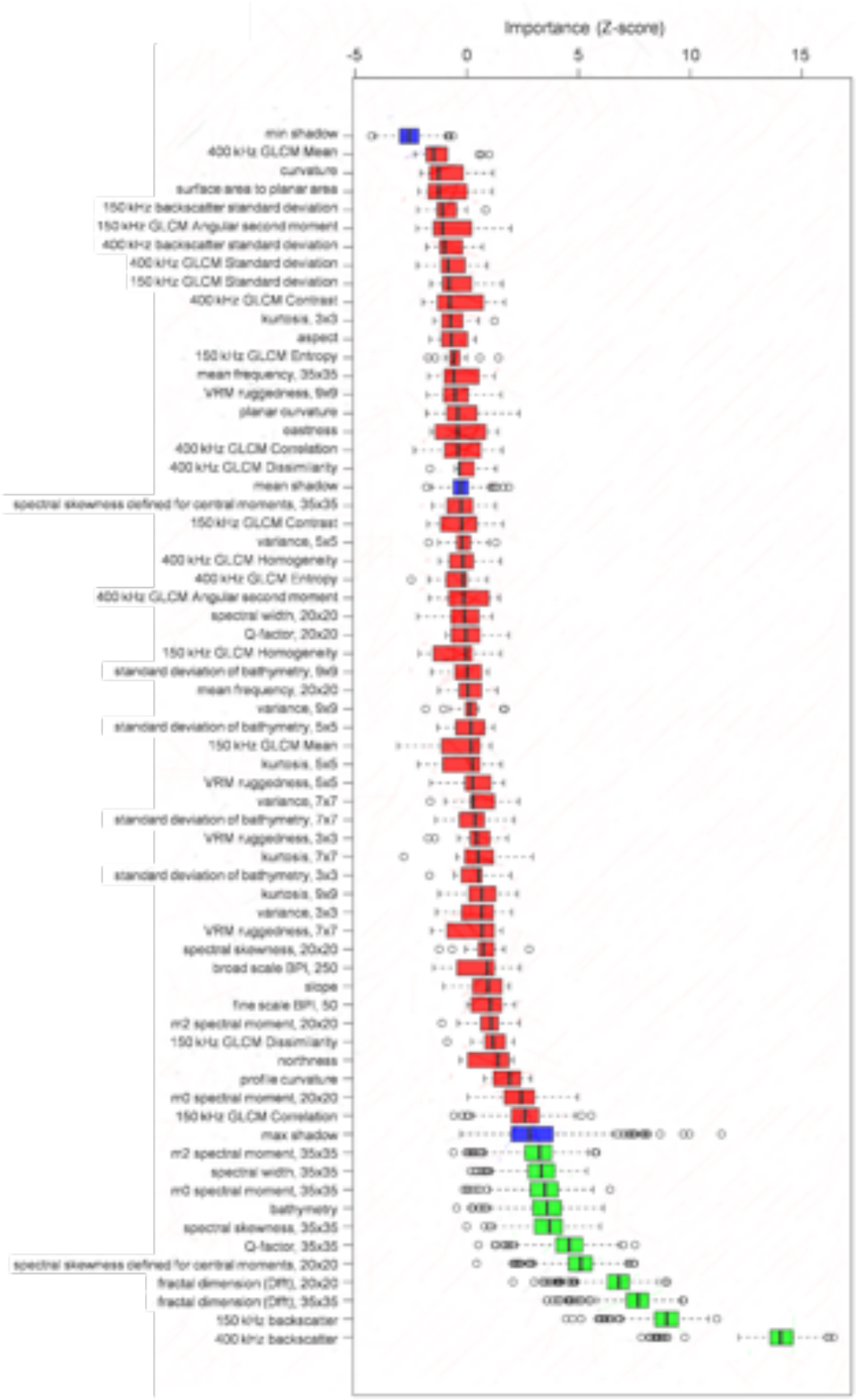

Fig. 4.1. Result of Boruta feature selection algorithm for all parameters used in this study.

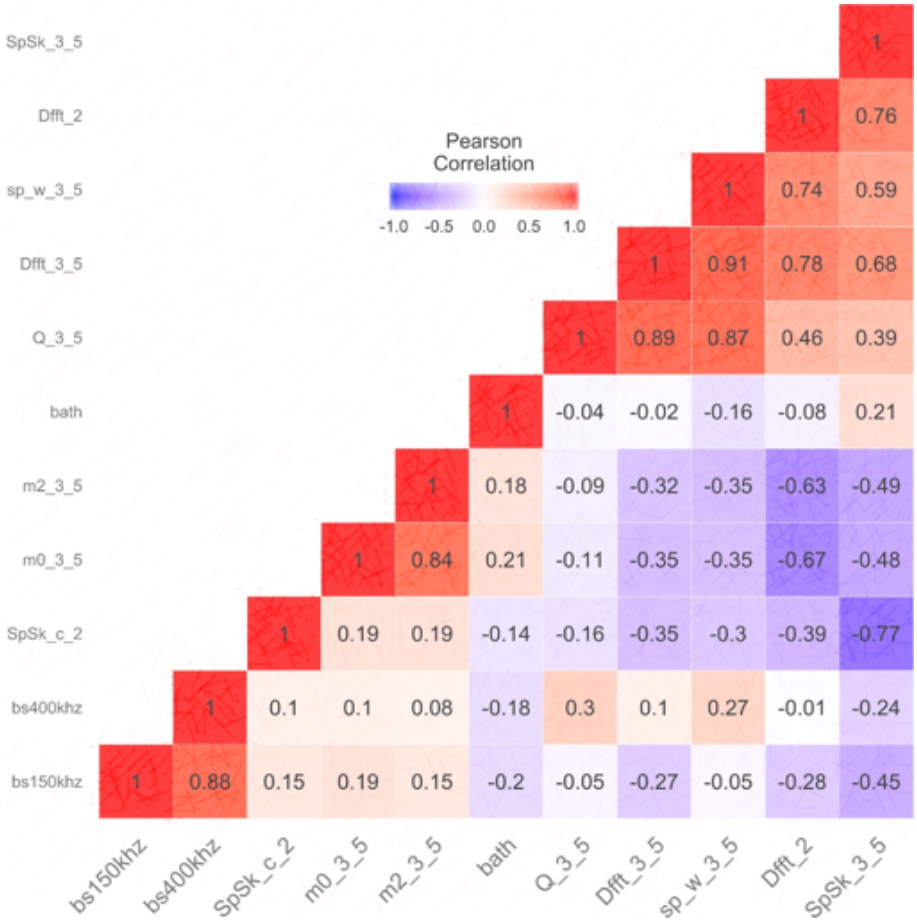

Fig. 4.2. Result of correlation matrix for features selected in this study (acronyms used: bs150khz – backscatter 150 kHz; bs400khz – backscatter 400 kHz; SpSk_c_2 - spectral skewness defined for central moments – 20; m0_3_5 - spectral moment m_0 (35); m2_3_5 - spectral moment m_2 (35); bath – bathymetry; Q_3_5 - Q-factor (35); Dfft_3_5 - fractal dimension (35); sp_w_3_5 - spectral width (35); Dfft_2 - fractal dimension (20); SpSk_3_5 - spectral skewness (35).

4.3 Image segmentation and classification

From twenty scales of multiresolution segmentation and four methods of supervised classification, the best classification performance was found for the MS 8 and SVM classifier. We adopted the following properties of the SVM classifier: radial-basis function kernel with C factor 100 and gamma 0.1. We created three predictive models using following sets of features: (1) all relevant; (2) uncorrelated, (3) only primary features (backscatter 400 kHz and bathymetry). The predictive benthic habitat maps generated using this approach are shown in Figure 4.3.

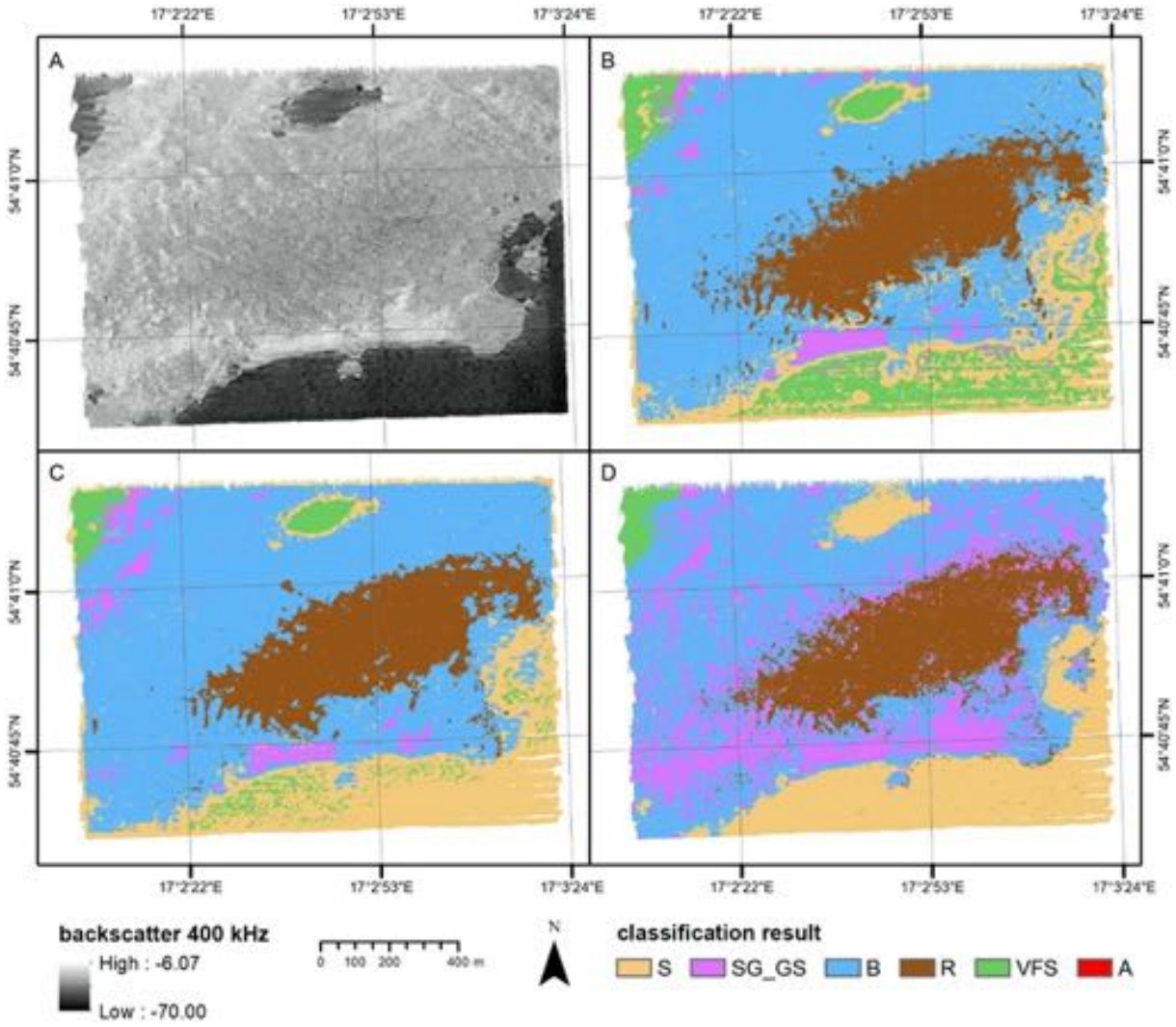

Fig. 4.3. Comparison between backscatter 400 kHz grid (A) and classification results for: all relevant features (B); uncorrelated features (C) only primary features (D). S - sand, B - boulders, R - red algae on boulders, SG_GS - sandy gravel or gravelly sand, VFS - very fine sand.

4.4 Accuracy assessment

The error matrix and accuracy assessment of the predictive habitat mapping method are presented in Table 2. Based on the validation subset of ground-truth samples, the model with all relevant features confirms a high performance reaching 86% prediction accuracy and a 0.82 Kappa index of agreement. The second model (considering only uncorrelated features) also reached high accuracy, but in comparison with the previous map, it misclassified one validation sample. The reference model without spectral features had the overall accuracy and Kappa index of agreement lower of more than 20% and 0.25 than the best model, respectively. Considering user's and producer's accuracy, the two highest models had very reasonable agreements for specific classes, like: VFS, S and R.

Table 2. Error matrices and accuracy assessment statistics for three benthic habitat models.

All relevant features		Reference					
		S	SG_GS	B	R	VFS	Sum
Prediction	S	7	0	0	0	0	7
	SG_GS	0	2	0	0	0	2
	B	1	2	7	1	0	11
	R	0	0	0	3	0	3
	VFS	0	0	0	0	5	5
	Sum	8	4	7	4	5	
	Producer's	0.875	0.5	1	0.75	1	
	User's	1	1	0.636	1	1	
	Overall Accuracy	0.857					
	KIA	0.815					
Uncorrelated		S	SG_GS	B	R	VFS	Sum
Prediction	S	6	0	0	0	0	6
	SG_GS	0	2	0	0	0	2
	B	2	2	7	1	0	12
	R	0	0	0	3	0	3
	VFS	0	0	0	0	5	5
	Sum	8	4	7	4	5	
	Producer's	0.75	0.5	1	0.75	1	
	User's	1.000	1.000	0.583	1	1	
	Overall Accuracy	0.821					
	KIA	0.769					
Only primary features		S	SG_GS	B	R	VFS	Sum
Prediction	S	6	0	0	0	2	8
	SG_GS	1	2	3	1	0	7
	B	1	2	4	0	0	7
	R	0	0	0	3	0	3
	VFS	0	0	0	0	3	3
	Sum	8	4	7	4	5	
	Producer's	0.75	0.5	0.571	0.75	0.6	
	User's	0.75	0.286	0.571	1	1	
	Overall Accuracy	0.643					
	KIA	0.545					

5. Summary

In this study we introduced eight spectral features of rough seafloor surface. The importance of spectral features was evaluated and expressed using importance score. We built and estimated accuracy of three models of benthic habitat mapping, showing that majority of introduced spectral features (7/8) may improve predictive power of supervised classifiers.

This study emphasizes the importance of spectral parameters derived from bathymetry for predictive benthic habitat mapping based on multibeam echosounder multi-frequency measurements. Because our study site is characterized by complex geomorphological features, we assume that the presented method of predictive benthic habitat mapping might be especially powerful in other areas with diverse morphology, like e.g. reefs. Considering a wider perspective, spectral analysis of the seafloor bathymetry may provide a new insight to DEM analysis from other sources allowing exploration and interpretation of large scale complex geomorphological features, like i.e. volcanic structures, seamounts or mid-ocean ridges.

References

- Benz, U. C., Hofmann, P., Willhauck, G., Lingenfelder, I., & Heynen, M. (2004). Multi-resolution, object-oriented fuzzy analysis of remote sensing data for GIS-ready information. ISPRS Journal of Photogrammetry and Remote Sensing, 58(3-4), 239-258. doi:10.1016/j.isprsjprs.2003.10.002
- Blaschke, T., Hay, G. J., Kelly, M., Lang, S., Hofmann, P., Addink, E., . . . Tiede, D. (2014). Geographic Object-Based Image Analysis - Towards a new paradigm. ISPRS J Photogramm Remote Sens, 87(100), 180-191. doi:10.1016/j.isprsjprs.2013.09.014
- Breiman, L., Friedman, J. H., Olshen, R. A., & Stone, C. J. (1984). Classification and Regression Trees. Belmont: Wadsworth.
- Breiman, L. (2001). Random Forests. Machine Learning, 45(1), 5-32. doi:10.1023/a:1010933404324
- Bremner, D., Demaine, E., Erickson, J., Iacono, J., Langerman, S., Morin, P., & Toussaint, G. (2005). Output-Sensitive Algorithms for Computing Nearest-Neighbour Decision Boundaries. Discrete & Computational Geometry, 33(4), 593-604. doi:10.1007/s00454-004-1152-0
- Calder, B.R.; Mayer, L.A. Automatic processing of high-rate, high-density multibeam echosounder data. Geochemistry, Geophysics, Geosystems 2003, 4, doi:10.1029/2002gc000486.
- Clough, R.W., Penzien, J., Dynamics of structure 1975, McGraw-Hill, New York.
- Cohen, J. (1960). A Coefficient of Agreement for Nominal Scales. Educational and Psychological Measurement, 20(1), 37-46. doi:10.1177/001316446002000104

- Cortes, C., & Vapnik, V. (1995). Support-vector networks. Machine Learning, 20(3), 273-297. doi:10.1007/bf00994018
- Congalton, R. G. (1991). A review of assessing the accuracy of classifications of remotely sensed data. Remote Sensing of Environment, 37(1), 35-46. doi:10.1016/0034-4257(91)90048-b
- Diesing, M., Green, S. L., Stephens, D., Lark, R. M., Stewart, H. A., & Dove, D. (2014). Mapping seabed sediments: Comparison of manual, geostatistical, object-based image analysis and machine learning approaches. Continental Shelf Research, 84, 107-119. doi:10.1016/j.csr.2014.05.004
- Folk, R. L., & Ward, W. C. (1957). Brazos River bar [Texas]; a study in the significance of grain size parameters. Journal of Sedimentary Research, 27(1), 3-26. doi:10.1306/74d70646-2b21-11d7-8648000102c1865d
- Fonseca, L., Brown, C., Calder, B., Mayer, L., & Rzhanov, Y. (2009). Angular range analysis of acoustic themes from Stanton Banks Ireland: A link between visual interpretation and multibeam echosounder angular signatures. Applied Acoustics, 70(10), 1298-1304. doi:10.1016/j.apacoust.2008.09.008
- Foody, G. M. (2002). Status of land cover classification accuracy assessment. Remote Sensing of Environment, 80(1), 185-201. doi:10.1016/s0034-4257(01)00295-4
- Haralick, R. M., Shanmugam, K., & Dinstein, I. H. (1973). Textural Features for Image Classification. IEEE Transactions on Systems, Man, and Cybernetics, SMC-3(6), 610-621. doi:10.1109/tsmc.1973.4309314
- Hasan, R., Ierodiaconou, D., & Monk, J. (2012). Evaluation of Four Supervised Learning Methods for Benthic Habitat Mapping Using Backscatter from Multi-Beam Sonar. Remote Sensing, 4(11), 3427-3443. doi:10.3390/rs4113427
- Janowski, L., Trzcinska, K., Tegowski, J., Kruss, A., Rucinska-Zjadacz, M., & Pocwiardowski, P. (2018). Nearshore Benthic Habitat Mapping Based on Multi-Frequency, Multibeam Echosounder Data Using a Combined Object-Based Approach: A Case Study from the Rowy Site in the Southern Baltic Sea. Remote Sensing, 10(12), 1983. doi:10.3390/rs10121983
- Kendzierska, H. Stilo-Ustka. In Atlas of Polish marine area bottom habitats, Gic-Grusza, G., Kryla-Straszewska, L., Urbanski, J., Warzocha, J., Weslawski, J.M., Eds. Broker-Innowacji: Gdynia, 2009; pp. 158-165.
- Kursa, M. (2016). Robust and efficient approach to feature selection with machine learning. University of Warsaw.
- Mandelbrot, B.B., The fractal geometry of nature, 1982, Freeman, San Francisco.
- Maritime Institute in Gdansk. Roznorodnosc biologiczna przybrzeznego glazowiska Rowy przy Slowinskim Parku Narodowym (Biodiversity of coastal boulder area near the Slowinski National Park, in Polish); Zaklad Wydawnictw naukowych Instytutu Morskiego w Gdansku: Gdansk, 2006.

- Misiuk, B., Lecours, V., & Bell, T. (2018). A multiscale approach to mapping seabed sediments. PLoS ONE, 13(2), e0193647. doi:10.1371/journal.pone.0193647
- Montereale Gavazzi, G., Madricardo, F., Janowski, L., Kruss, A., Blondel, P., Sigovini, M., & Foglini, F. (2016). Evaluation of seabed mapping methods for fine-scale classification of extremely shallow benthic habitats – Application to the Venice Lagoon, Italy. Estuarine, Coastal and Shelf Science, 170, 45-60. doi:10.1016/j.ecss.2015.12.014
- Nilsson, R., Peña, J. M., Björkegren, J., & Tegnér, J. (2007). Consistent Feature Selection for Pattern Recognition in Polynomial Time. Journal of Machine Learning Research, 8, 589-612.
- Parnum, I. M., & Gavrilov, A. N. (2011). High-frequency multibeam echo-sounder measurements of seafloor backscatter in shallow water: Part 2 – Mosaic production, analysis and classification. Underwater Technology, 30(1), 13-26. doi:10.3723/ut.30.013
- Sappington, J. M., Longshore, K. M., & Thompson, D. B. (2007). Quantifying Landscape Ruggedness for Animal Habitat Analysis: A Case Study Using Bighorn Sheep in the Mojave Desert. Journal of Wildlife Management, 71(5), 1419-1426. doi:10.2193/2005-723
- Schimel, A. C. G., Beaudoin, J., Parnum, I. M., Le Bas, T., Schmidt, V., Keith, G., & Ierodiaconou, D. (2018). Multibeam sonar backscatter data processing. Marine Geophysical Research, 39(1-2), 121-137. doi:10.1007/s11001-018-9341-z
- Story, M., & Congalton, R. G. (1986). Accuracy assessment: A user's perspective. Photogrammetric Engineering and Remote Sensing, 52, 397-399.
- Tegowski, J., Gorska, N., Kruss, A., Nowak, J., & Blenski, J. (2009). Analysis of single beam, multibeam and sidescan sonar data for benthic habitat classification in the southern Baltic Sea. Paper presented at the 3rd International Conference and Exhibition on Underwater Acoustic Measurements: Technologies & Results, Nafplion, Greece.
- Tegowski, J., Trzcinska, k., Kasprzak, M., Nowak, J., (2016), Statistical and spectral features of corrugated seafloor shaped by the Hans glacier in Svalbard, Remote Sensing 8 (9), 744.
- Walbridge, S., Slocum, N., Pobuda, M., & Wright, D. (2018). Unified Geomorphological Analysis Workflows with Benthic Terrain Modeler. Geosciences, 8(3), 94.
- Wentworth, C. K. (1922). A Scale of Grade and Class Terms for Clastic Sediments. The Journal of Geology, 30(5), 377-392.
- Wilson, M. F. J., O'Connell, B., Brown, C., Guinan, J. C., & Grehan, A. J. (2007). Multiscale Terrain Analysis of Multibeam Bathymetry Data for Habitat Mapping on the Continental Slope. Marine Geodesy, 30(1-2), 3-35. doi:10.1080/01490410701295962